

## **GITM-Data Comparisons of the Depletion and Enhancement during the 2017 Solar Eclipse**

Chen Wu<sup>1,2</sup>, A. J. Ridley<sup>2</sup>, Larisa Goncharenko<sup>3</sup>, Gang Chen<sup>1</sup>

<sup>1</sup> Electronic Information School, Wuhan University, Wuhan, Hubei, China.

<sup>2</sup> Climate and Space Sciences and Engineering, University of Michigan, Ann Arbor,  
Michigan, USA.

<sup>3</sup> Haystack Observatory, Massachusetts Institute of Technology, Westford, MA, USA

Corresponding author: Aaron Ridley, Climate and Space Sciences and Engineering,  
University of Michigan, Ann Arbor, Michigan, USA. (ridley@umich.edu)

### **Key Points:**

- Model-data comparisons showed a relatively consistent depletion and enhancement in the ionosphere during and after the eclipse
- GITM showed that the divergence of horizontal winds drove the increased O after the eclipse allowing an increase in the ionization rate
- Slower charge exchange due to both the decreased ion temperature and N<sub>2</sub> density allowed an increase of O<sup>+</sup> density in the F-region also

This is the author manuscript accepted for publication and has undergone full peer review but has not been through the copyediting, typesetting, pagination and proofreading process, which may lead to differences between this version and the [Version of Record](#). Please cite this article as doi: [10.1002/2018GL077409](https://doi.org/10.1002/2018GL077409)

**Abstract**

The total solar eclipse of August 21, 2017 was simulated with the Global Ionosphere-Thermosphere Model (GITM), and the results were compared with the total electron content (TEC) measurements provided by the Global Navigation Satellite System (GNSS), as well as F2 layer peak electron density (NmF2) derived from six ionosondes. TEC decreased over North America by ~54.3% in the model and ~57.6% in measurements, and NmF2 decreased by ~20-50% in the model and ~40-60% in the measurements. GITM predicted a post-eclipse enhancement of ~10% in TEC and NmF2, consistent with observations which suggested an increase of ~10-25% in TEC and ~10-40% in NmF2. GITM showed that the divergence of horizontal winds drove the increase in Oxygen after the eclipse allowing an increase in the ionization rate. The slower charge exchange due to both the decreased ion temperature and N<sub>2</sub> density allowed an increase of O<sup>+</sup> density in the F-region also.

**1. Introduction**

Numerous studies have been conducted to investigate the electron density ( $N_e$ ), electron ( $T_e$ ) and ion ( $T_i$ ) temperatures, gravity waves, irregularities, electric fields, etc. during solar eclipse events [e.g., Rishbeth, 1968, Chimonas and Hines, 1970, Jakowski et al., 2008]. The locally direct ionospheric response includes the decrease of the electron and ion temperatures due to lack of the extreme ultraviolet (EUV) heating, as well as the depletion of the electron densities resulting from the reduction of the photo-ionization. Studies have shown that the density below the F layer decreases substantially, while the net ionization in the F layer may decrease slightly, remain unchanged, or even increase during the solar eclipse, depending on the competing effects of the loss in photo-ionization and the diffusion above the F2 peak [e.g., Boitman et al., 1999; Le et al., 2009; Ding et al., 2010]. Neutral composition and neutral winds also play a crucial role in the ionospheric response to the eclipse [Le et al., 2008; Müller - Wodarg and Aylward, 1998; Madhav Haridas and Manju, 2012; St.-Maurice et al., 2011, etc.].

A solar eclipse provides a good opportunity to test thermosphere-ionosphere models' response to the impulse variations of solar EUV over a limited region of the Earth, and the models can help to understand the unclear phenomena and mechanisms during the events. However, while an extensively large number of observational studies have been conducted to investigate the ionospheric response to solar eclipses,

there are only a few modeling studies [Roble et al., 1986; Salah et al., 1986, etc.]. Earlier simulations that lacked realistic boundary conditions, eclipse function, etc. did not match observations well and therefore needed improving [Korenkov et al., 2003a, 2003b; Müller - Wodarg and Aylward, 1998, etc.]. The Theoretical Ionospheric Model of the Earth in Institute of the Geology and Geophysics, Chinese Academy of Sciences (TIME-IGGCAS), was used to simulate the mid-latitude ionospheric response to solar eclipses over South and East Asia. It was found that due to the large plasma flux from the topside ionosphere, the TEC response around 30°N was mainly due to the electron density response below 200 km [Le et al., 2010]. Pitout et al. (2013) reproduced common features of the ionospheric response to a high-latitude eclipse over EISCAT Svalbard Radars with the 1-D TRANSCAR model that describes the dynamics of different ionospheric species along a magnetic field line. Huba and Drob (2017) applied SAMI3, a global ionosphere and plasmasphere model, to predict the ionospheric response to the August 21, 2017 solar eclipse quantitatively. It was indicated that the electron density decreased by 50% in the F region with O<sup>+</sup> velocities changing from 40 m/s upward to 20 m/s downward.

The enhancement associated with the solar eclipse has been reported by both observational and simulational studies, but most of them were during the eclipse, especially during the first phase [e.g., Evans, 1965a; Anastassiades and Moraitis, 1968;

Cheng et al., 1992]. The during-eclipse enhancement is thought to result from the downward diffusion of ions due to the lowering of equilibrium scale height caused by a large drop in  $T_e+T_i$  in the F region [Evans, 1965b; Boitman et al., 1999]. Compared to the enhancement during the eclipse, post-eclipse enhancement is rare and the physical processes are not clear. Chen et al. (2013) reported a post-eclipse enhancement due to downward transport from the plasmasphere after analyzing electron profiles at middle latitudes. Huang et al (1999) suggested that the post-eclipse enhancement in TEC was due to the daily variations of the equatorial ionization anomaly (EIA) at low latitudes, while Tsai and Liu (1999) theorized that the solar eclipse induced a strengthened pre-reversal enhancement resulting in the post-eclipse enhancement. Simulations with the Coupled Thermosphere-Ionosphere-Plasmasphere Model (CTIP) indicated that the enhanced  $[O]/[N_2]$  ratio contributed to the electron density enhancement after the eclipse, and Korenkov et al. (2003b) suggested that the decrease of  $N_2$  due to cooling was the driver of the enhancement of the F2 layer critical frequency ( $f_oF_2$ ).

In this letter, we present simulation results of the Global Ionosphere-Thermosphere Model (GITM), as well as the observations from GPS receivers and six ionosondes (see Figure 3) distributed in North and South America. The simulated response of TEC and  $NmF_2$  were consistent with observations,

especially an enhancement after the eclipse which was not reproduced by Huba and Drob (2017), who made the simplifying assumption that neutral thermospheric feedback effects were negligible. Detail analysis showed that the divergence of the horizontal winds caused drove the increase in Oxygen after the eclipse allowing an increase in the ionization rate. The slower charge exchange due to both the decreased ion temperature and  $N_2$  density allowed an increase of  $O^+$  density in the F region also.

## 2. Methodology

The Global Ionosphere-Thermosphere Model (GITM) is a 3-D first-principles model, which allows different models of high-latitude electric fields, auroral particle precipitation, solar EUV inputs, and particle energy deposition to be used [Ridley et al., 2006]. During a solar eclipse, the Moon obscures the disk of the Sun and thus the solar EUV input into the upper atmosphere decreases in the limited region around the totality. In order to determine the path and mask for the eclipse, the coordinates of the GITM grid ( $X, Y, Z$ ) were converted into the GSE (Geocentric Solar Ecliptic) system ( $X_{GSE}, Y_{GSE}, Z_{GSE}$ ), based on the local time, latitude, and solar declination angles. It was assumed that the Moon casts a circular shadow in the ( $Y_{GSE}, Z_{GSE}$ ) coordinates, while the  $X_{GSE}$  of the grid points was assumed to be much smaller than the Earth-moon distance, such that the size of the occulted region was constant. Figures 1(a) and

(b) show the linear path of the center of the totality region in the GSE and Geographic coordinate systems and the path from a NASA website ([https://informal.jpl.nasa.gov/museum/sites/default/files/ResourceLibrary/2017\\_eclipse\\_path.kml](https://informal.jpl.nasa.gov/museum/sites/default/files/ResourceLibrary/2017_eclipse_path.kml)). The NASA points do not make a perfectly straight line in GSE coordinates, while here it is approximated as one. The root-mean-square difference between the linear approximation and the NASA points is 14.7 km, which is significantly smaller than the grid cells in GITM. The occultation within GITM was calculated using the distance between the GITM grid point and the center of the totality in the  $(Y_{GSE}, Z_{GSE})$  plane. Figure 1(c) shows the percentage of the nominal EUV heating and ionization that occurred in the GITM cells as a function of distance away from the center point of the eclipse. It was assumed within GITM that the region of the mask has two stages: near the edge, the brightness decreased exponentially, while near the center, the brightness decreased linearly.

To validate the simulation results of the ionosphere, the global TEC and the NmF2 data from six ionosondes were analyzed. The TEC data were provided by the International GNSS Service Ionosphere Working Group with 15-minute time resolution (<https://cdaweb.sci.gsfc.nasa.gov/index.html/>). The NmF2 data were derived from the ionograms provided by the Digital Ionogram Database (DIDBase) and were manually scaled via the interactive ionogram scaling software (Reinisch et

al., 2009). The time resolution of NmF<sub>2</sub> presented in this work was 15 minutes in North America and 10 minutes in South America.

### 3. Results and Discussion

The lunar umbra initiated contact with North America on the west coast at approximately 16:00 UT, and left the continent at approximately 20:00 UT on the east coast. Figure 2 shows the percentage differences of TEC between the eclipse and reference days. Figure 2(a) shows the difference between GITM simulation results with and without the eclipse. The red line represents the path of the eclipse and the red triangle is the umbra of the Moon at the moment that is labelled at the top of each sub-plot. Figure 2(b) is similar to Figure 2(a), except it shows the GPS observations, with the baseline reference being the average of 10 quiet days ( $K_p < 4$ ): 5 days before and 5 days after the eclipse. Both simulations and observations showed a depression during and after the eclipse. In terms of the depression during the eclipse, the temporal and spatial variations were consistent in general. The depletion began in the northwest of North America at ~17:00 UT when the totality began. The depression then expanded and propagated southeast. At ~18:30 UT, the ionosphere above almost the entire United States was depressed. This depression then shifted southeast, eventually recovering gradually after the end of the eclipse and lingering until the end



of the day, although the simulated depletion disappeared more rapidly. Quantitatively, the depletion in GPS TEC was ~30-40% at 17:00 UT and reached a maximum of ~57.6% at about 18:30 UT, while the depression in the model was ~40-50% at 17:00 UT and a maximum was ~54.3% at 18:30. Coster et al. (2017) also showed difference variations of GPS TEC with Aug 29, 2017 as the reference day during the same eclipse event. The temporal and spatial variations of the depletion were consistent with the observational and modeling results here, though they showed a larger decrease exceeding 60%. This discrepancy might be caused by the different selection of the reference day.

Figures 3(a)- 3(d) show NmF2 perturbations derived from four ionosondes in North America. The locations of the ionosondes are denoted by black triangles in the TEC maps in Figure 2. For each station, after the start of the eclipse, the simulated NmF2 began to decrease, reached the minimum after the totality of the eclipse, and then gradually recovered. The maximum reduction in each of the four locations were ~23.1%, ~40.0%, ~46.3%, and ~34.9% in GITM, and ~42.6%, ~58.3%, ~48.8%, and ~44.3% from observations. Essentially, the simulations were consistent with the observations, though the observations showed a slower recovery from the eclipse, while the GITM results showed a much more rapid recovery. The observations may also have shown a slight lag between when the totality occurred and when the

minimum in NmF2 occurred, while GITM did not indicate an obvious lag. Just after the end of the eclipse, the NmF2 was still lower than the background at all the stations, although several hours later at three of the stations, the NmF2 became higher than the average.

Figures 3(e) and 3(f) show comparisons between the simulation and observations at two stations in South America. The observational NmF2 was enhanced well before the eclipse, and revealed an increase during, as well as after the eclipse, while the simulated NmF2 showed little change, although extremely minor differences occurred after about 19 UT. Since the umbra of the Moon did not reach South America, it is difficult to say whether these observed variations were associated with the eclipse.

GITM predicted a post-eclipse enhancement in North America associated with the solar eclipse with TEC and NmF2 increased by ~10%. In Figure 2(a), the TEC enhancement began in the west at approximately 19:30 UT (not shown here), and then spread southeast along the totality path of the eclipse. About two hours later, the enhancement overcast the entire United States. Accordingly, in Figures 3(a)- 3(d), GITM showed enhanced NmF2 at all of the four locations after the eclipse. In Boulder (40°N, 254.7°E) and Idaho (43.8°N, 247.3°E) which were closer to the totality of the eclipse, NmF2 was increased by ~10%, while in Austin (30.4°N, 262.3°E) and Millstone Hill (42.6°N, 288.5°E) which were relatively far from the

totality, NmF2 was increased less than 10%. This enhancement agreed relatively well with the measurements. In Figure 2(b), from 21:00 UT to 23:00 UT, the GPS TEC was enhanced by ~10-25% in the United States. The enhancement also started from the west of the continent and then evolved along the totality path until it covered the entire region that was depressed during the main phase of the eclipse. In Figures 3(a)-3(d), the NmF2 was increased up to ~30-40% in Boulder and Idaho and ~10% in Millstone Hill after approximately 22:00 UT. And Austin didn't show a clear increase in NmF2 after the solar eclipse. Though all geomagnetic effects cannot be excluded in the observations, based on the comparisons with model and associations with the totality path, it appears likely that the enhancement recorded by the measurements was caused by the eclipse. Note that the variance was very large at 22 UT, indicating that the reference days may not have been very quiet.

The continuity equation of ions may help to determine what caused the density increase, and can be written as [Schunk and Nagy, 2000]:

$$\frac{\partial N_i}{\partial t} + \nabla \cdot (N_i \mathbf{V}_i) = S - L \quad (1)$$

where  $N_i$  is the number density of the ions,  $\mathbf{V}_i$  is the velocity of ions,  $S$  is the production rate, and  $L$  is the loss rate. The source of the enhancement could be due to advection, changes in production, or recombination processes. Evans (1965b) investigated six ionosondes distributed in Alaska, Canada, and North America

revealing an enhancement of  $foF2$  during the first phase of the eclipse. He suggested that the downward diffusion of ions resulted in the increase of electron density. Chen et al. (2013) used measurements from a network of ionosondes showing an enhancement after the solar eclipse on 15 January 2010. The electron density profiles indicated that a downward plasma flux from the plasmasphere was the driver. At low-latitudes, the variations of the electron density may have been associated with the pre-reversal enhancements lifting the ionosphere from below [Tsai and Liu, 1999]. Müller-Wodarg and Aylward (1998) suggested that an electron density enhancement after an eclipse was related to the neutral composition (enhanced  $[O]/[N_2]$  ratio) with the Coupled Thermosphere-Ionosphere-Plasmasphere Model (CTIP). Korenkov et al. (2003b) modeled the 11 August 1999 solar eclipse and compared  $foF2$  with experimental data. An enhanced  $foF2$  after the eclipse could be discerned, which was suggested to be driven by a decrease of  $N_2$  due to cooling.

GITM is not coupled with a plasmasphere, and Huba and Drob (2017) did not reproduce the post-eclipse enhancement with the ionosphere-plasmasphere model, therefore the downward diffusion of ions is most likely not the source during this particular eclipse, even though there was a strong change in  $T_e$ . Also, the enhanced region was too far away from the EIA to be affected by the electrojets. Figures 4(a)-4(g) show simulated variations of neutral temperature, ion temperature, neutral

vertical wind, zonal wind, meridional wind,  $N_2$  density and O density at 300 km in Idaho (43.8°N, 247.3°E). At the onset of the eclipse, the neutral temperature, as well as the ion and electron (not shown) temperatures, decreased dramatically. The upward vertical neutral wind reversed direction due to the lowering of pressure, while both the westward and northward winds increased after the totality. The downwelling of the pressure level decreased the neutral density at a fixed altitude [Müller-Wodarg and Aylward, 1998], although the individual species variation differed due to the different gradients involved. After the maximum obscuration, the neutral temperature started to recover and the atmosphere began to expand. Simultaneously, the O and  $N_2$  densities started to increase towards the non-eclipse state, however, the O density was enhanced above the non-eclipse case after and even before the end of the eclipse, while the  $N_2$  density was still lower than the expected value after the eclipse, driving an increased  $[O]/[N_2]$  ratio. In the F region, the  $O^+$  ions are mainly produced by the ionization of O, and lost due to charge exchange with  $N_2$ . The increase of the  $[O]/[N_2]$  ratio therefore was likely to be the source of the enhanced electron density after the eclipse.

The different dynamics of O and  $N_2$  are puzzling. The vertical continuity equation for each species is:

$$\frac{\partial N_n}{\partial t} = -N_n \nabla \cdot \mathbf{V}_n - \mathbf{V}_n \cdot \frac{\partial N_n}{\partial r} \quad (2)$$

where  $N_n$  and  $V_n$  are the number density and the vertical velocity of the neutral species respectively,  $-N_n \nabla \cdot V_n$  is the divergence term, and  $-V_n \cdot \frac{\partial N_n}{\partial r}$  is the advection term. The total of the divergence term and advection term determines the change of density. Based on equation (2), the rate of change of O and N<sub>2</sub> density were calculated in both vertical and horizontal directions. The integral of the rate of change caused by the different terms was also calculated. Figures 4(h)- 4(j) show the density differences caused by different terms for O and N<sub>2</sub> between runs with and without the eclipse as a function of time at 300 km in Idaho (43.8°N, 247.3°E). In the vertical direction (blue lines), the divergence term (4h) contributed a slight increase of O and N<sub>2</sub>, while the advection term (4i) drove a substantial decrease in the density. Therefore, in the vertical direction (blue lines), the total for O and N<sub>2</sub> (4j) was decreased by  $\sim 0.8 \times 10^{14}/\text{m}^3$  and  $\sim 0.4 \times 10^{14}/\text{m}^3$  during the eclipse and started to recover before the end of the eclipse. Consequently, if only the vertical direction was considered, both the O and N<sub>2</sub> densities would have decreased though out the eclipse, taking several hours to recover. In the horizontal direction (red lines), the divergence term (4h) was dominated for both O and N<sub>2</sub>, while the advection term (4i) was quite small. These two terms together (4j) resulted in an increase of O by  $\sim 0.9 \times 10^{14}/\text{m}^3$  and N<sub>2</sub> by  $\sim 0.3 \times 10^{14}/\text{m}^3$  after the beginning of the solar eclipse. The sum of the total in the vertical and horizontal direction showed that the O and N<sub>2</sub> decreased at the onset of

the eclipse, then started to recover after the totality. However, the O was enhanced before the end of the eclipse, while N<sub>2</sub> remained lower than the non-eclipse state. For O, the minimum of the depression was  $\sim -0.3 \times 10^{14}/\text{m}^3$  while the maximum was  $\sim -0.2 \times 10^{14}/\text{m}^3$ . The divergence in the horizontal wind caused the increase in Oxygen after the eclipse. When the eclipse started, the decrease of the temperature caused the decrease in the pressure, resulting in the contraction of the atmosphere and the convergence of winds. The downward winds led the decrease of the density. As the horizontal winds accelerated away from their nominal behavior, a convergence in the winds started to develop. Because the density of O was much larger than the density of N<sub>2</sub>, the horizontal convergence term in O became larger than vertical downwelling, resulting in a net increase in O, while N<sub>2</sub> continued to be lower than nominal conditions.

In addition to the enhanced O density, the ion temperature (4b) and the N<sub>2</sub> density (4g) were decreased both during and after the eclipse. Both the ion temperature and the N<sub>2</sub> density play a strong role in the charge exchange rate between O<sup>+</sup> and N<sub>2</sub>, the main loss mechanism in the F<sub>2</sub> ionosphere. The decreased ion temperature reduced the charge exchange rate constant [Torr and Torr, 1978], while the decreased N<sub>2</sub> would have directly reduced the loss rate, which may have contributed to the enhanced electron density after the eclipse.

#### 4. Conclusions

We have simulated the total solar eclipse of August 21, 2017 with the Global Ionosphere-Thermosphere Model (GITM) and compared the results with GPS TEC, as well as NmF<sub>2</sub> derived from six ionosondes. The conclusions we have made from the simulation and data-model comparisons are:

1. A direct decrease of TEC was revealed by both the model and measurements with consistent temporal and spatial variations. The TEC was reduced by ~54.3% in the model and ~57.6% in measurements, while the NmF<sub>2</sub> was decreased by ~20-50% in the model and ~40-60% in measurements. The fact that the simulated TEC was consistent with measurements and NmF<sub>2</sub> was underestimated during the solar eclipse might be due to the lack of a plasmasphere in GITM. After the eclipse, the depression shifted southeast recovering gradually and lingered until the end of the day.
2. A post-eclipse enhancement that was not reproduced by SAMI3, which ignored neutral thermospheric feedback effects, was discerned after ~21:00 UT over the United States where the TEC increased by ~10% in GITM and ~10-25% in the measurements, and NmF<sub>2</sub> increased by ~10% in GITM and ~10-40% in the measurements which is likely to be caused by enhanced [O]/[N<sub>2</sub>] ratio due to different dynamics of O and N<sub>2</sub>, as well as decreased ion temperature.



3. Detail analysis of the terms in the continuity equation indicated that the divergence in the horizontal wind drove the increase in Oxygen after the eclipse allowing an increase in the ionization rate. The slower charge exchange caused by both the decreased ion temperature and  $N_2$  density allowed an increase of  $O^+$  density in the F region also.

### **Acknowledgments**

The NOAA Space Weather Prediction Center provided the interplanetary magnetic field data and solar wind data of the NASA Advanced Composition Explorer (ACE) satellite, as well as the F10.7 index. This paper also used ionospheric data from the Digisonde network, TEC data from the International Global Navigation Satellite Systems (GNSS) Service Ionosphere Working Group. Model results and input files, and GITM code are available upon request, while the GITM code is available on GitHub. One of the test cases contains the parameters to set up the eclipse simulation. This research was supported by AFOSR under DDDAS (Dynamic Data-Driven Applications Systems <http://www.1dddas.org/>) grant FA9550-16-1-0071, and partially funded by NASA NNX14E046 and NSF 1452097. L. Goncharenko was partially supported by NASA grant NNX17AH71G. We thank Douglas Drob for his helpful discussion and providing example files of the EUV mask, allowing the creation of the

geometric mask used within the study.

## References

- Anastassiades, M., and G. Moraitis (1968), On the behavior of foF2 during the 20 May 1966 solar eclipse, *J. Atmos. Terr. Phys.*, 30(8), 1471–1478, doi:10.1016/S0021-9169(68)90191-8.
- Boitman, O. N., A. D. Kalikhman, and A. V. Tashchilin (1999), The mid- latitude ionosphere during the total solar eclipse of March 9, 1997, *J. Geophys. Res.*, 104(A12), 28, 197–28, 206.
- Chen, G., et al. (2013), Nighttime ionospheric enhancements induced by the occurrence of an evening solar eclipse, *J. Geophys. Res. Space Physics*, 118, 6588–6596, doi:10.1002/jgra.50551.
- Chen, G., C. Wu, X. Huang, Z. Zhao, D. Zhong, H. Qi, L. Huang, L. Qiao, and J. Wang (2015), Plasma flux and gravity waves in the midlatitude ionosphere during the solar eclipse of 20 May 2012, *J. Geophys. Res. Space Physics*, 120, 3009–3020, doi:10.1002/2014JA020849.
- Cheng, K., Y. - N. Huang, and S. - W. Chen (1992), Ionospheric effects of the solar eclipse of September 23, 1987, around the equatorial anomaly crest region, *J. Geophys. Res.*, 97(A1), 103 – 111, doi:10.1029/91JA02409.

Chimonas, G., and C. O. Hines (1970), Atmospheric gravity waves induced by a solar eclipse, *J. Geophys. Res.*, 75(4), 875–875, doi:10.1029/JA075i004p00875.

Coster, A. J., Goncharenko, L., Zhang, S.-R., Erickson, P. J., Rideout, W., & Vierinen, J. (2017). GNSS observations of ionospheric variations during the 21 August 2017 solar eclipse. *Geophysical Research Letters*, 44, 12,041–12,048. <https://doi.org/10.1002/2017GL075774>

Ding, F., et al. (2010), GPS TEC response to the 22 July 2009 total solar eclipse in East Asia, *J. Geophys. Res.*, 115, A07308, doi:10.1029/2009JA015113.

Evans, J. V. (1965a), An F region eclipse, *J. Geophys. Res.*, 70(1), 131 – 142.

Evans, J. V. (1965b), On the behavior of foF2 during solar eclipses, *J. Geophys. Res.*, 70(3), 733–738.

Huang, C. R., C. H. Liu, K. C. Yeh, K. H. Lin, W. H. Tsai, H. C. Yeh, and J. Y. Liu (1999), A study of tomographically reconstructed ionospheric images during a solar eclipse, *J Geophys. Res.*, 104(A1), 79-94.

Huba, J. D., and D. Drob (2017), SAMI3 prediction of the impact of the 21 August 2017 total solar eclipse on the ionosphere/plasmasphere system, *Geophys. Res. Lett.*, 44, 5928–5935, doi:10.1002/2017GL073549.

Jakowski, N., Stankov, S. M., Wilken, V., Borries, C., Altadill, D., Chum, J., ... Cander, L. R. (2008). Ionospheric behavior over Europe during the solar eclipse

of 3 October 2005. *Journal of Atmospheric and Solar-Terrestrial Physics*, 70(6), 836–853.

Korenkov, Y. N., V. V. Klimenko, V. Baran, I. I. Shagimuratov, and F. S. Bessarab (2003a), Model calculations of TEC over Europe during 11 August 1999 solar eclipse, *Adv. Space Res.*, 31(4), 983–988.

Korenkov, Y. N., V. V. Klimenko, F. S. Bessarab, N. S. Nutsvalyan, and I. Stanislawska (2003b), Model/Data comparison of the F2-region parameters for the 11 August 1999 solar eclipse, *Adv. Space Res.*, 31(4), 995–1000.

Le, H., et al. (2010), Observations and modeling of the ionospheric behaviors over the east Asia zone during the 22 July 2009 solar eclipse, *J. Geophys. Res.*, 115, A10313, doi:10.1029/2010JA015609.

Le, H., L. Liu, X. Yue, and W. Wan (2008), The midlatitude F2 layer during solar eclipses: Observations and modeling, *J. Geophys. Res.*, 113, A08309, doi:10.1029/2007JA013012.

Le, H., L. Liu, X. Yue, W. Wan, and B. Ning (2009), Latitudinal dependence of the ionospheric response to solar eclipses, *J. Geophys. Res.*, 114, A07308, doi:10.1029/2009JA014072.

Madhav Haridas, M. K., and G. Manju (2012), On the response of the ionospheric F region over Indian low-latitude station Gadanki to the annular solar eclipse of 15

January 2010, *J. Geophys. Res.*, 117, A01302, doi:10.1029/2011JA016695.

Müller - Wodarg, I. C. F., A. D. Aylward, and M. Lockwood (1998), Effects of a mid - latitude solar eclipse on the thermosphere and ionosphere —A modelling study, *Geophys. Res. Lett.*, 25(20), 3787 - 3790, doi:10.1029/1998GL900045.

Pitout, F., P.-L. Blelly, and D. Alcaydé (2013), High-latitude ionospheric response to the solar eclipse of 1 August 2008: EISCAT observations and TRANSCAR simulation, *J. Atmos. Terr. Phys.*, 105-106, 336–349, doi:10.1016/j.jastp.2013.02.004

Reinisch, B. W., et al. (2009), New Digisonde for research and monitoring applications, *Radio Sci.*, 44, RS0A24, doi:10.1029/2008RS004115.

Ridley, A., Y. Deng, and G. Tòth (2006), The Global Ionosphere-Thermosphere Model, *J. Atmos. Sol. Terr. Phys.*, 68, 839–864.

Rishbeth, H. (1968). Solar eclipses and ionospheric theory. *Space Science Reviews*, 8, 543–554.

Roble, R. G., B. A. Emery, and E. C. Ridley (1986), Ionospheric and Thermospheric Re- sponse Over Millstone Hill to the May 30, 1984, Annular Solar Eclipse, *Journal of Geo- physical Research*, 91(5), 1661-1670, doi:5A8748.

Salah, J. E., W. L. Oliver, J. C. Foster, J. M. Holt, B. A. Emery, and R. G. Roble (1986), Observations of the May 30, 1984, annular solar eclipse at Millstone Hill,

Journal of Geophysical Research, 91(A2), 1651, doi:10.1029/JA091iA02p01651.

St. - Maurice, J. - P., K. M. Ambili, and R. K. Choudhary (2011), Local electrody-  
namics of a solar eclipse at the magnetic equator in the early after- noon hours,  
Geophys. Res. Lett., 38, L04102, doi:10.1029/ 2010GL046085.

Schunk, W. R., and A. F. Nagy (2000), Ionospheres: Physics, Plasma Physics, and  
Chemistry, pp. 606–607, Cambridge Univ. Press, Cambridge, U. K.

Torr, D. G., and M. R. Torr (1978), Review of rate coefficients of ionic reactions  
determined from measurements made by the Atmosphere Explorer satellites, Rev.  
Geophys., 16, 327–340.

Tsai, H. F. and J. Y. Liu (1999), Ionospheric total electron content response to solar  
eclipses, J. Geophys. Res., 104(A6), 12657-12668.

**Figure 1.** The path of the center of totality in GSE (a) and geographic coordinates (b). The solid lines indicate the linear path as described here; the triangles indicate the NASA specified locations of the totality. The stars in (a) indicate the linear path at the same times as the triangles. The percentage of the total EUV heating and ionization in GITM as a function of distance from the center of totality(c). The solid line indicates the total percentage change; the dashed line indicates just the linear portion.

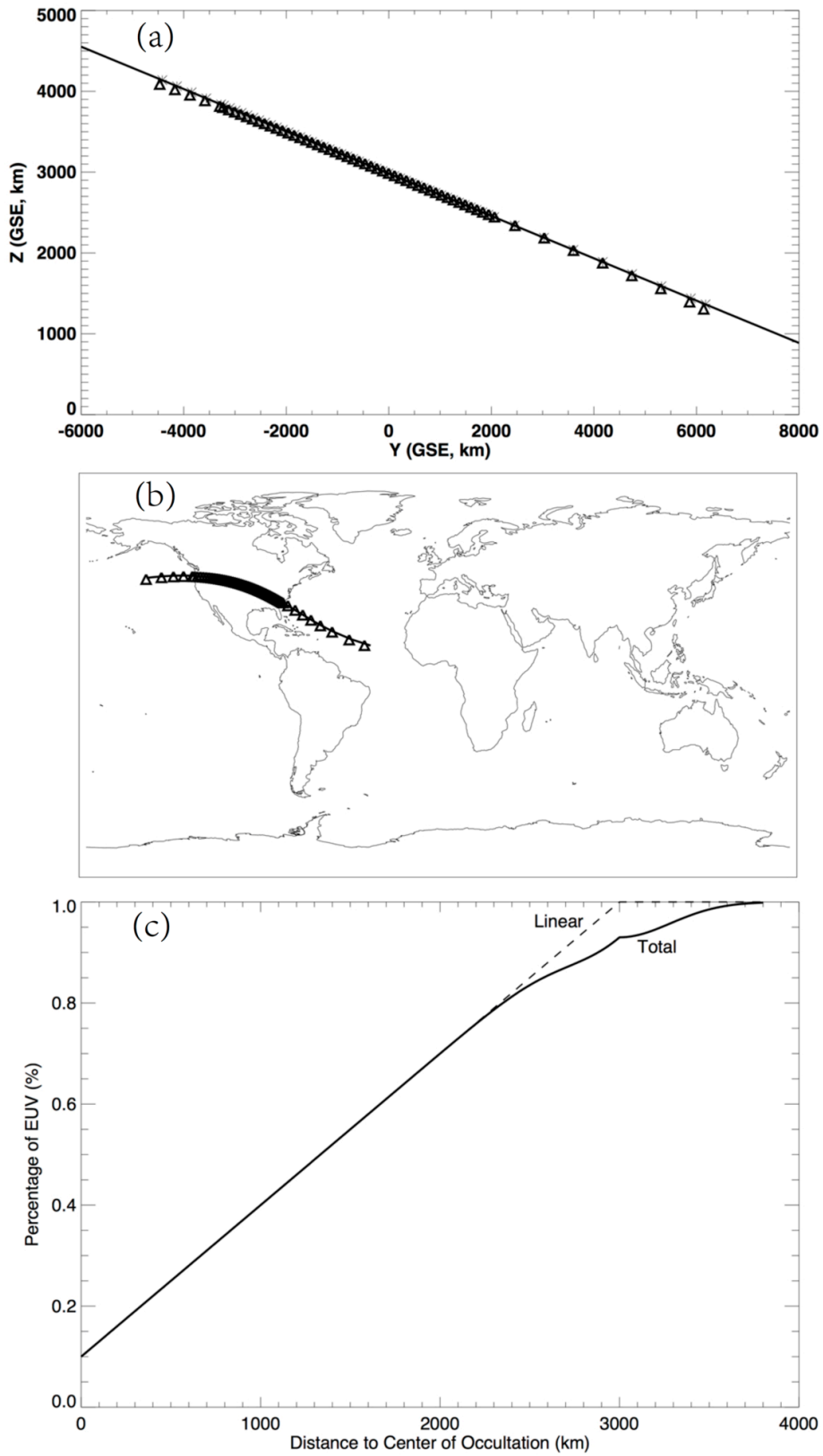
**Figure 2.** Percentage difference of TEC from GITM(a) and GPS(b) with the solar eclipse path (red solid line) and the totality at the moment (red triangle).

**Figure 3.** NmF2 in GITM with (blue solid line) and without (blue dashed line) eclipse and in measurements on August 21 (red line) and reference days (black line) as a function of UT hours in North America (a-d) and South America (e, f). The gray error bars represent one standard deviation. The three dashed grey lines are the start, the max obscuration, and the end of the total eclipse, respectively.

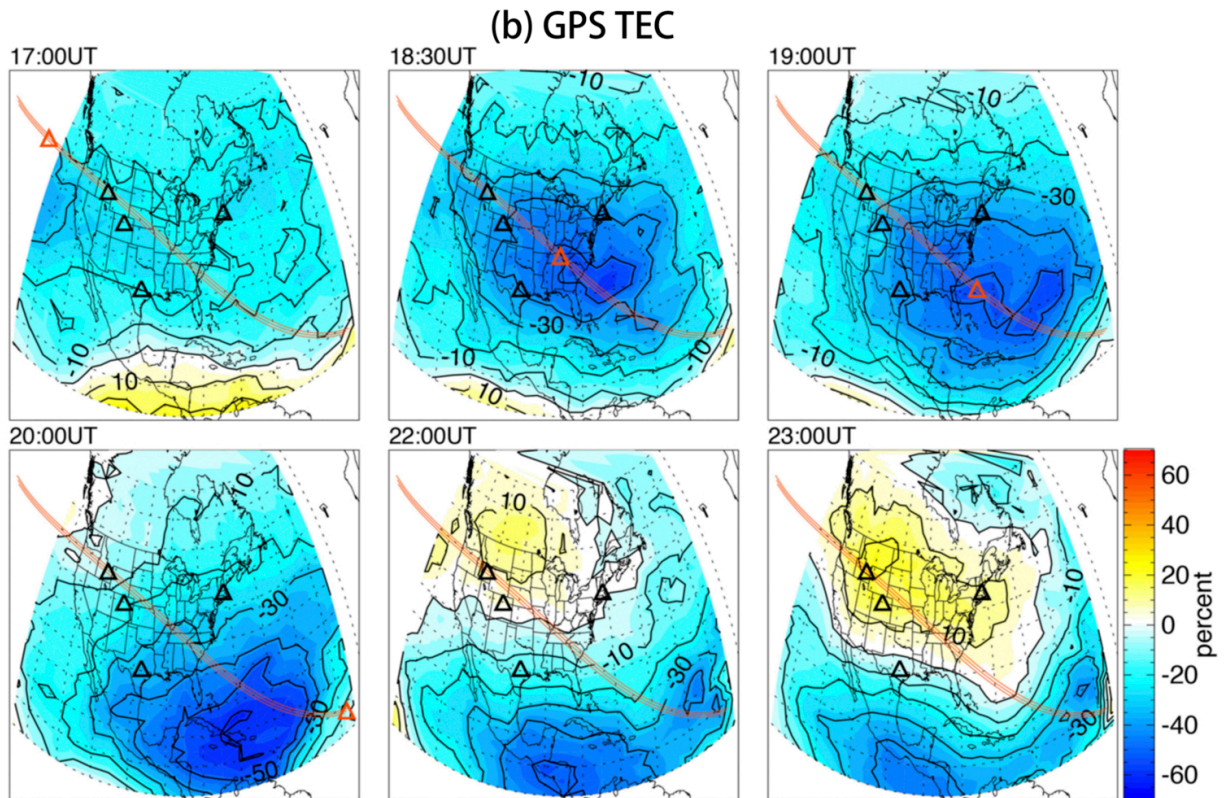
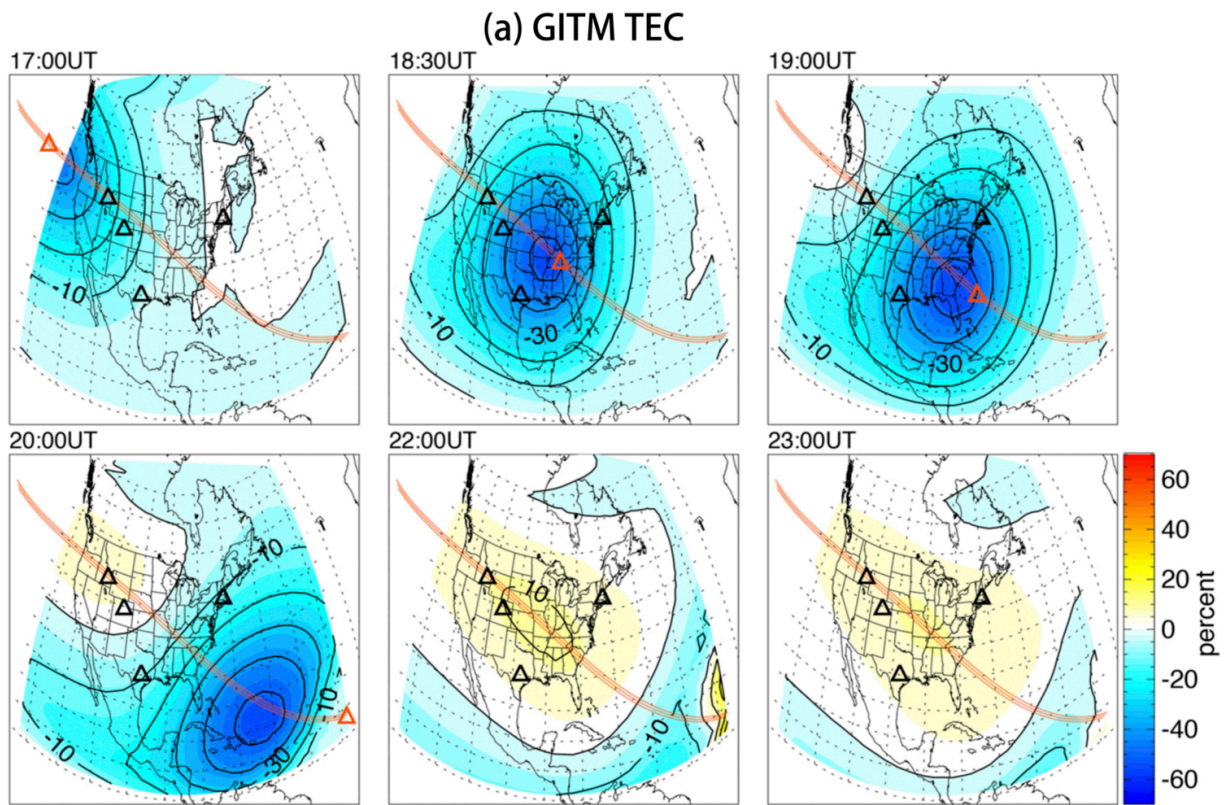
**Figure 4.** Simulated neutral temperature (a), ion temperature (b), neutral vertical wind (c), zonal wind (d), meridional wind (e), N<sub>2</sub> density (f) and O density (g) with (solid line) and without eclipse (dashed line) as a function of UT hours; density difference of

O (solid lines) and N<sub>2</sub> (dashed lines) between runs with and without eclipse as a function of UT hours derived from the divergence term (h), advection term (i) and total (j) in the continuity equation for the vertical (blue lines), horizontal direction (red lines) and total of the two directions (black lines).

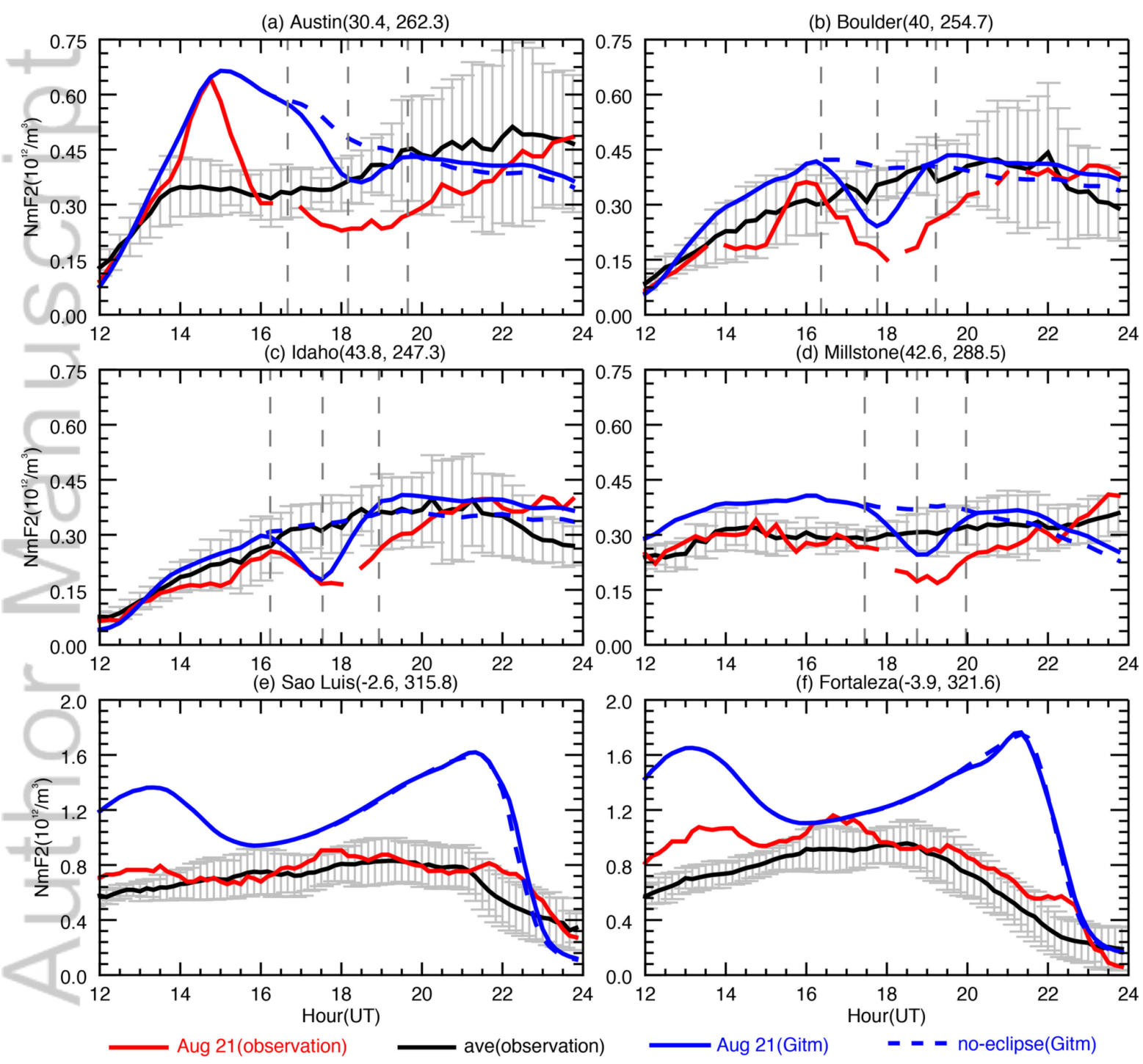




2018GL077409-f01-z-.png

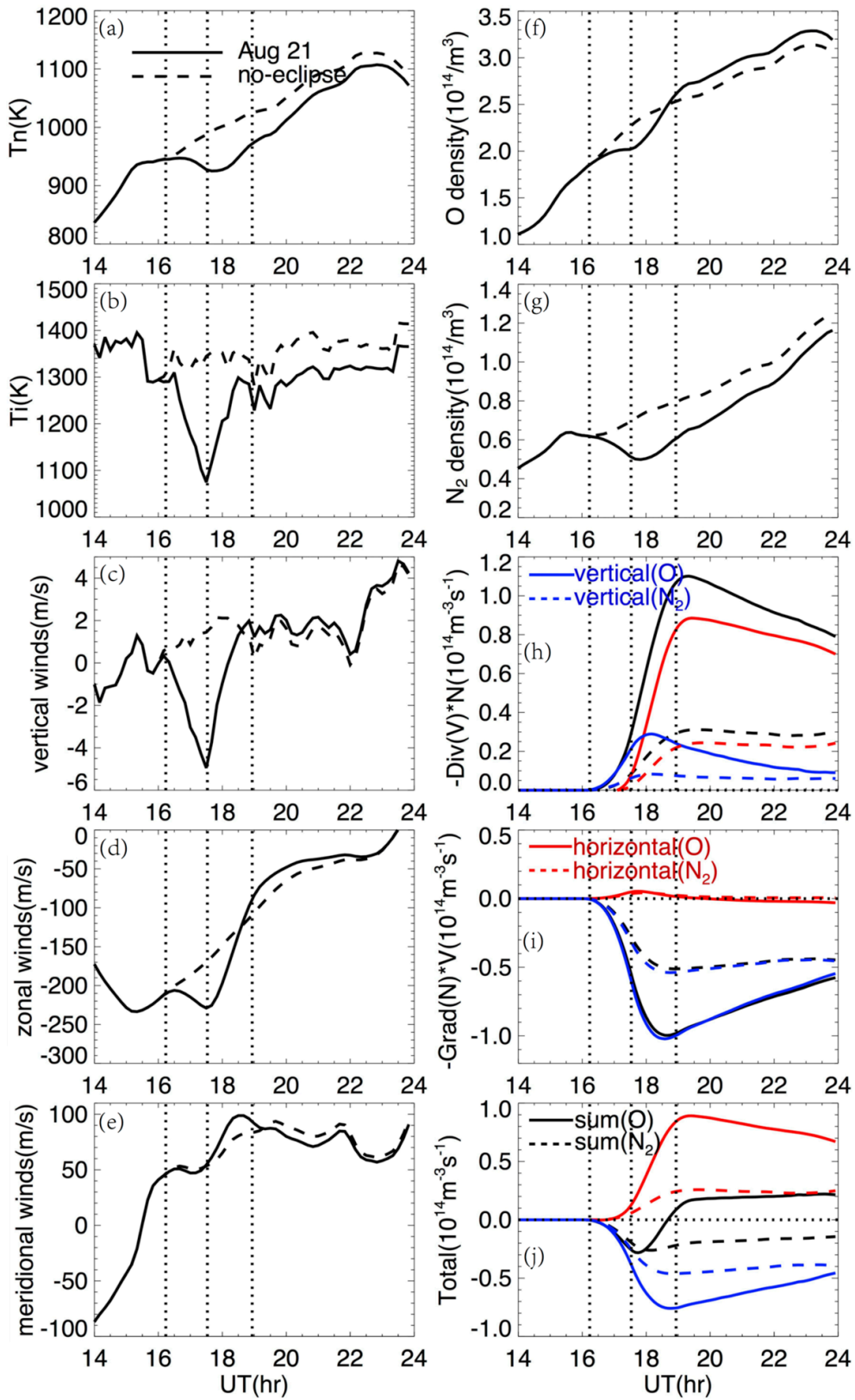


2018GL077409-f02-z.png



2018GL077409-f03-z-.png





2018GL077409-f04-z-.png